APPLICATION OF PARTICAL IMAGE VELOCIMETRY IN REINFORCED CONCRETE PILE CAP EXPERIMENTS

Jing Cao[1] Alan G Bloodworth[2]

Author details
Author 1
J. Cao BSc PhD ***(Corresponding author)***
Senior Structural Engineer, Structural Division,
Heavy Engineering Research Association
17-19 Gladding Place, Manukau,
Auckland 2241
New Zealand
Email: jing.cao@hera.org.nz

Author 2
A.G. Bloodworth MA MSc DIC DPhil CEng MICE
Principal Teaching Fellow, School of Engineering, Univ. of Warwick
Library Road,
Coventry CV4 7AL
U.K.
Tel: 023 8059 3947
Fax: 023 8067 7519
Email: a.bloodworth@warwick.ac.uk

ABSTRACT: *Particle image velocimetry (PIV) is an optical method to measure full-field displacement of moving objects, with significant advantages over traditional method using labour intensive strain gauges. This paper introduces an application of PIV with single non-commercial digital camera, in a series of reinforced concrete four-pile cap shear experiments performed by the first author at University of Southampton, the UK during his PhD study. The PIV measurement for cap surface displacement and strain distribution helped to reveal the shear behaviour of reinforced concrete pile caps under wall loadings. A full PIV procedure and the derivation of displacement/strain data from PIV readings is explained.*

This paper also presents an error analysis for the inherent random and system errors associated with PIV technology. Advice are made regarding the efficient way to improve the measurement accuracy for future implementation. Examples of the corrected output from PIV are given and compared with numerical modelling output.

Keywords: Photogrammetry, PIV, pile-cap, reinforced concrete, FEA, digital camera

Notations

d	Resultant displacement = $\sqrt{u^2 + v^2}$
E_c	Young's modulus of concrete
E_s	Young's modulus of steel
f_{cu}	Concrete cube compressive strength
f_t	Concrete tensile strength
f_y	Yield strength of reinforcement
IA	Interrogation area
r_u, r_v	System error correction factor for horizontal and vertical displacements
R	Scale factor between length in mm in object co-ordinates and length in pixels in image co-ordinates
SA	Search area
TA	Target area
(u, v)	Horizontal and vertical displacements in object co-ordinates (mm)
(x, y)	Horizontal and vertical co-ordinates in object co-ordinates (mm)
(U', V')	Horizontal and vertical displacement in image co-ordinates (pixels)
(Δx, Δy)	Horizontal and vertical base lengths for calculation of strain (mm)
ε^{cr}	Crack strain
ε^{e}	Limiting tensile elastic strain
ε_1	Maximum principal strain
$\varepsilon_{xx}, \varepsilon_{yy}$	Horizontal and vertical direct strains

Introduction

Photogrammetry applies an algorithm of image recognition to compare two digital images taken before and after the movement of a target area. Merits of photogrammetry over traditional point-based measuring methods such as strain gauges are its non-contact full-field measurement of the displacement and strain on the target area, and its economics in terms of time and labour cost. Previous experience of its use on reinforced concrete (RC) structures includes investigation of several beams subjected to shear failure. Displacement on the concrete surface was obtained by tracing a set of target square tags, combined with a recognition system [1][2][3].

Particle image velocimetry (PIV) was first used in fluid mechanics to measure flow velocity by seeding a flow with mica particles, taking two consecutive exposures on one light sheet or traditional film, and then constructing an image intensity field inside a series of interrogation volumes. A correlation could then trace and record the maximum movement of the interrogation volumes [4]. As such, the technique is not limited to just tracking the movement of discrete targets.

With modern digital technology and software, PIV has gained higher efficiency and reliability and a large number of different implementations exist for varying applications. Digital PIV using a single camera has been used to measure large strain sand deformations around a driven pile [5]. However, its application in small strain RC deformation is relatively uncommon. This paper describes its application using a single non-commercial camera in a series of experiments on RC pile caps in shear [6]. It proved possible to obtain the full-field incremental displacement and strain distribution between two loading steps, subject to a certain level of errors. The outputs are validated against direct readings of displacement and are compared against finite element analysis (FEA) models of the experimental samples. Strain in the longitudinal reinforcement closest to the cap surface was obtained using PIV and used to confirm the occurrence of strut-and-tie shear behaviour.

Principles of the PIV method for RC surface measurement

Mathematical base

Digital images are taken of the subject at two different loading steps. Within both images, a *target area* (TA) (for example, the front surface of the pile cap) is defined, and in the first image sub-divided into *interrogation areas* (IA) (Fig. 1). The objective is to obtain the displacement of the centre of each IA in the second image. This is done by defining in the second image a *search area* (SA) for each IA in the first image and searching within this area for the best location for the IA from the first image. This best location is obtained using a statistical correlation method by which the tricolour value (red, green and blue, each ranging between 0 to 255) in each pixel in the IA in the first image is compared with the corresponding pixel in every possible IA of the same size occurring in a search area in the second image [7]. The location of the IA in the second image with the highest correlation coefficients for each tricolour value is used to calculate its displacement. Displacement vectors to more accurate sub-pixel level are obtained by interpolating displacement vectors with peak and sub-peak correlation coefficients. Repeating the process for every IA in the target area in the first image gives the approximately the full-field displacement field, which can be differentiated to obtain full-field strains.

The processing of the digital images in this project was performed using a MATLAB-based program GeoPIV8 [8] which used normalized cross-correlation and two-dimensional spatial Hermite bicubic surface interpolation to obtain the displacement vector to sub-pixel accuracy [9].

Small strain assumption and strain output

In contrast to the large strain assumption such as made for soil deformation around a driven pile [5], small strain was assumed for the RC surface. Thus the horizontal and vertical direct strains, and shear strains, are as follows:

$$\varepsilon_{xx} = \frac{\Delta u}{\Delta x} \qquad (1)$$

$$\varepsilon_{yy} = \frac{\Delta v}{\Delta y} \qquad (2)$$

$$\gamma_{xy} = \gamma_{yx} = \frac{\Delta u}{\Delta y} + \frac{\Delta v}{\Delta x} \qquad (3)$$

Where Δu and Δv are the difference in horizontal and vertical displacements between IAs with horizontal and vertical spacings Δx and Δy respectively, the base lengths for strain calculation.

The principal strains can be calculated as follows:

$$\varepsilon_{1,2} = \frac{\varepsilon_{xx} + \varepsilon_{yy}}{2} \pm \sqrt{\left(\frac{\varepsilon_{xx} - \varepsilon_{yy}}{2}\right)^2 + \left(\frac{\gamma_{xy}}{2}\right)^2} \quad (4)$$

Application of PIV to pile cap experiments

Description of experiments

A series of experiments on reduced-scale pile caps in shear under full-width wall loading were carried out in Heavy Structures Laboratory at University of Southampton, the UK, on a total of 17 samples in four batches[6][10]. The experimental setup is shown in Figure 2. The caps were singly reinforced uniformly along cap soffit in orthogonal directions. The caps were loaded by uniform load increments until the onset of yield, after which displacement control was used. The applied load was recorded continuously, along with deflection of the cap top surface soffit by means of an array of 15 linear potentiometers. Cracks on the front surface were highlighted by hand and their propagation recorded as the test proceeded. Data from the tests was used to validate a numerical model which was further used in a parametric study to create data to improve design guidance for shear capacity of pile caps [11].

Hardware for PIV application

A standard non-commercial Olympus digital camera with 2288×1712 pixel resolution (4.0 Megapixel) was set up to capture an image of the front surface of the pile cap at each load increment (Fig. 2(b)). It was assumed that out-of-plane displacement of the cap front surface was not significant, so a single camera was sufficient. However, this required the camera's lens plane to be as parallel as possible to the concrete surface, achieved by mounting the camera on a heavy-based tripod positioned on the centre line of the pile cap, and rotating it about its horizontal and vertical axes until the cap appeared centrally in the image.

To capture consecutive digital images with the same optical settings (focus, aperture and zoom), Olympus camera control software was used. Operation of the camera was done remotely by the software and the images transmitted directly to the computer. Without manually touching the camera, the camera was undisturbed, the distance between the camera and cap surface was almost same in each test (from 1.8 m to 1.85 m, Fig. 2(b)) and so these optical settings were adjusted to give the clearest image and kept identical for each sample.

Concrete surface features

Whereas the texture of soil naturally has high tricolour contrast, the surface of normal concrete has low contrast between dark and light features (Fig. 3(a)). Therefore, an artificial pattern was painted on the concrete using a natural sponge dipped with black paint and dabbed on the surface. The softness and deformability of the natural sponge was found to give satisfactory random surface features and the use of black paint gave high contrast between dark and light areas (Fig. 3(b)).

Determination of PIV parameters

The definitions of the IA size and IA spacing in the first image, and size of the SA in the second image are shown in Figure 1. The challenge of choosing IA size is to make it small enough to capture detailed displacement information on a surface that may be cracked, whilst large enough that there are sufficient distinct surface features within the IA to reduce random errors to an acceptable level. It was found by trial that surface features (for example a black spot) should be at least 3 x 3 pixels in size and that there should be at least three such features in each IA for random errors to be acceptably low.

If a SA in the second image is intersected by a new crack which forms during the load increment, excessive noise in the displacement output often occurs. Ideally therefore, IAs should be placed each side of a crack but not intersected by it. The size of SA should be larger than the maximum possible translation of an IA in any direction that occurred between the first image (in this research the first loading step) and the second image (the final failure step or the onset of the yield stage). Considering the above, the IA array parameters and SA size chosen for the experimental samples in Batches 3 and 4 [6] (a total of 12 samples) are given in Table 1.

Transformation between image and object co-ordinates

Displacements of the concrete surface are output from GeoPIV8 in pixel units in an image co-ordination system with origin being at the top left of the target area, *x*-direction horizontal and *y*-direction vertically downwards (Fig. 1). The displacement vector in pixel units, relative to the fixed reference point where the load is applied on the top of the specimen, is (U', V').

To obtain the ratio R, the scaling factor between displacements in pixel units in image co-ordinates and in mm units on the physical samples in object co-ordinates (u, v), a survey levelling staff was included along the bottom

of the image and a 50 mm gauge length used to obtain the conversion between pixels and millimetres[6]. It was then assumed *R* was equal in both directions and constant over the whole field of view of the camera. *R* obtained for all samples was found to be around 0.700 mm/pixel.

(*U'*, *V'*) is further corrected to take account of system errors in displacement by means of the factors r_u, r_v which are close to 1.0 as discussed below. Thus the resulting vector of displacements (*u*, *v*) in millimetres relative to the fixed loading point, which can be compared with the FEA output, is given by:

$$u = U' \times R \times r_u \quad (5)$$

$$v = V' \times R \times r_v \quad (6)$$

System and random errors and error correction

Introduction

Errors are inherent in a technique such as photogrammetry. The performance of a measuring system can be assessed by means of its *accuracy* and its *precision*. Accuracy is defined as the systematic difference or the system error between a measured quantity and the true value. Precision is related to the random difference or the random error between multiple measurements of the same object [1]. The standard deviation (STD) of the random error is taken to represent the level of the precision.

In the case of PIV, system error stems from non-planarity between the lens plane and the plane of the target surface, lens and CCD distortion and pixel non-squareness (i.e. the physical partition on the CCD is not strictly square) [7]. Most of these cause error during the capture of the object into image co-ordinates. Random error results from camera resolution, the non-uniform distribution of features on the object surface, and the methodology in the processing software (e.g. GeoPIV8) by which displacements of the IAs are obtained. With a particular digital camera chosen, error from the latter is related to the choice of IA and SA sizes relative to feature size on the target area [1] which was studied below.

System error can be corrected for through a camera calibration to obtain a matrix transforming co-ordinates in object space to image space. Random error may be reduced by careful choice of PIV parameters, by multiple measurements or by improvement in camera resolution. In this research, system and random error were assessed by means of a simple 'pre-test' for each experimental specimen in which a known vertical rigid-body displacement was applied.

Uniform displacement 'pre-test'

During the pre-test, each sample was given several vertical displacements without loading. The true displacement was recorded by the test machine and by a suitably located dial gauge. The case of cap B4B3 to which a maximum displacement expected *V'* = -5.5477 pixels was applied is now discussed.

The sensitivity of the error in the PIV results to different combinations of IA (20 pixels, 40 pixels and 60 pixels) and SA size (10 pixels and 60 pixels) was investigated. IA spacing was kept constant at 16 pixels (representing the level of detail in the full-field displacements that was desired by the user).

It is important to note that the pre-test gives the random error in displacements for a population of IAs in an array within one shot rather than for a single IA in multiple shoots. Thus the random error obtained will be related to the distribution of the features on the concrete surface, rather than other causes such as lighting changes that occur between shoots.

Displacement errors

Cap B4B3 was chosen as an example. The co-ordinate system and the array of IAs is shown in Figure 4. Uncorrected vertical and horizontal displacements *U', V'* from digital PIV in pixel units for B4B3 in the pre-test are shown in Figures 5 and 6. There are 10 rows and 42 columns of IAs in the target area.

The random error can be seen in Figures 5 and 6 as an oscillation of the PIV results about the regression lines. The mean and STD of *U', V'* is shown in Table 2. The difference between the regression lines themselves and the real value of displacement is the system error. The regression lines being non-horizontal, e.g. the parabolic regression line shown in Figure 6 for *V'* ($y=5E\text{-}07x^2\text{-}0.0003x\text{-}5.8913$), is due to the camera lens non-planarity and distortion.

Strain error (dummy strain)
From the pre-test displacement results, non-zero random error incurred strain measurement ε_{xx}, ε_{yy} (Eqns. 1 and 2) was obtained using a 64 pixel base length in both directions (i.e. length roughly covering 5 IAs with 4 intervals of 16 pixels). Mean and STD of random strain ε_{xx}, ε_{yy} is shown in Table 3.

Non-zero system error incurred strain can be obtained by differentiating the regression lines, e.g. as shown in Figure 5 that for *U'* regression line y=-0.0003x-0.0664 indicates constant horizontal compression strain ε_{xx} of -0.0003 along IA Rows 5 and 6 (Figure 4).

Because in reality there was no strain on the concrete surface, this strain caused by the system and random errors is termed the 'dummy strain'.

Minimisation for random error in displacement and strain
Influence of IA and SA sizes on random errors in *U', V'* in pixels, ε_{xx} and ε_{yy} was investigated by means of the STD of the pre-test PIV results shown in Tables 2 and 3. Random error is relatively independent of SA size. The variation against IA size for random error incurred displacement (*u*, *v*) in mm and strain is shown in Figures 7 and 8 for SA of 10 pixels. The trend is for random error to decrease with increasing IA size, albeit at a gradually decreased rate. Thus apart from increasing the camera resolution, the most efficient way to reduce the random error in displacement and strain is to increase IA size, although this comes at a cost of processing time. As the original purpose of the PIV application to the pile cap project was to study shear behaviour at failure with large strain value expected, an IA size of 20 x 20 pixels was selected at benefit of savings on processing time.

The minimum STD of the displacement the GeoPIV8 applied on soil material can reach is ± 0.01 pixels [5]. From Table 2 this figure is taken to be ± 0.05 pixels for concrete surface. Taking this figure, the precision on calculated strain is of the order $\pm 0.05/64 = 780\mu\varepsilon$ (c.f. Table 3). Assuming a concrete compressive strength f_{cu}=20MPa, tensile strength f_t=2MPa and Young's modulus E_c= 28 GPa, the tensile cracking strain would be 2/28000 = 71 με and the strain at the compressive yielding point of the order of -20/28000 = 710 με. This means that neither tensile strain prior to cracking nor the onset of concrete compressive yielding can be observed accurately in this case.

Compensation for system error in displacement
Compensation factors r_u and r_v in Eqns 5 and 6 are defined as the ratios of the true horizontal and vertical displacements to the regression lines of the recorded *U', V'* (see Figures 5 and 6). Because only vertical displacements could be applied in the pre-test, it is assumed that $r_u = r_v$.

Theoretically, r_v varies over the field of view and with real displacement magnitude. For simplicity, the mean value (see Figures 5 and 6) was calculated and applied to the whole image. Table 3 shows the values of r_v thus obtained for various caps for different IA sizes, all of which are close to 1.0.

Compensation for system error in strain
The compensation of systematic errors caused by lens non-planarity and distortion was not considered due to the magnitude of dummy strain being much less than the expected large concrete strain at shear failure in critical tension and compression regions, e.g. the compression zone under loading and the tension strain along the bottom reinforcement.

Validation of PIV output in experiments
For cap B4A5 (Figure 9), which experienced compressive splitting shear at failure [6], Figure 10 shows the contours of maximum principal strain ε_1 (Eqn. 4) obtained from PIV and Figure 11 shows the crack strain ε^{cr} obtained from smear crack based FEA [6] at failure. Good agreement in the distribution of strain and cracking is seen. Because for concrete the limiting elastic strain in tension, ε^e, is much less than the typical crack strain ε^{cr}, the maximum principal strain $\varepsilon_1(=\varepsilon^e+\varepsilon^{cr})$ should approximate well to the crack strain ε^{cr} on the concrete surface.

Figure 12 compares ε_1 between PIV and FEA along the horizontal section $A-A$ shown Figures 10 and 11. The form of the graphs in terms of the general trends and positions of the strain peaks are similar. It was apparent from the experiment that failure and growth of major cracking was concentrated on the right side of the front surface in shear failure[6], hence the high peak in strain recorded there by PIV.

The reason for the difference in the peak strain value between PIV and FEA is given below. Smear crack based FEA assumes average crack width therefore local high crack width may be underestimated and provides stiffer response than PIV. However, PIV is capable of capturing real crack distribution thus concentrated crack strain near major shear splitting cracks was recorded.

Figure 13 shows contour of maximum horizontal strain ε_{xx} (Eqn. 1) for cap B4B2 at failure. The major feature is captured by PIV including that along the bottom longitudinal reinforcement, it can be seen that peak ε_{xx} (0.025~0.03) is located near bottom tip of major cracks, indicating yielding of the longitudinal reinforcement with yield strain of 0.0026 (=f_y/E_s=547MPa/210000MPa [6]).

Figures 14 and 15 compare resultant displacement $d = \sqrt{u^2 + v^2}$ (u,v derived from Eqns 5 and 6) obtained from PIV and FEA for the cap B4A5. Figure 16 plotted along the line $A - A$ again shows a similar trend. Different values again was due to FEA predicting a stiffer response than recorded by PIV. This comparison suggests that a smear crack based FEA may not well predict deformation of caps with individual major shear cracks at failure.

Conclusions

This paper describes a PIV application on non-contact measurement for concrete displacement and strain. Single non-commercial digital camera was implemented and data was processed by non-commercial program GeoPIV8. Full-field distribution of displacement and strain information on cap surface was successfully captured with peak concrete strain measured validated well with FEA. A detail error analysis was carried out and effort was taken to minimize the adverse influence from system and random errors on the PIV results. The study indicates a relatively low cost PIV equipment (in magnitude of $1000) is achievable with acceptable errors in lieu of purchasing high end professional commercial single or dual digital camera and analysis software package (normally priced above $10000).

Although digital camera with maximum resolution available on the market was purchase for the project (4.0 Megabytes back to year 2004), this still made PIV measurement incapable of measuring accurately the small concrete strain due to certain random errors incurred, e.g. at the loading stages before major cracks appeared. It is highly anticipated by using a digital camera with higher resolution (i.e. higher volume of pixels covered in an IA), which is now conveniently approachable, random errors can be significantly reduced in full field measurement tests with similar scale. For reference, a further study at University of Southampton which was based on this pile cap study, but with a 14.6 Megabyte non-commercial digital camera successfully detected timber batten strain at magnitude of 0.10με[12].

In this study, a standard procedure of error minimization and compensation with simplified dealing with system errors was introduced. In future application, it is suggested a full matrix correction function covering full cap surface be established to correct system errors within displacement and strain in both horizontal and vertical directions.

Acknowledgements

The authors are grateful to the Engineering and Physical Sciences Research Council (EPSRC) for the project funding under Grant Ref. GR/S17888/01, and to David White of the University of Cambridge for making available the program GeoPIV8 and giving much helpful advice on its use.

References

1. Qu, Z., Lu, X.Z., Ye, L.P., and Chen, J. (2006). Application of the Digital Photogrammetry in the Studies. *Journal of Building Structures*, 936-939.
2. Jeppsson, J. (2000). Contact-free Monitoring of Cracked Concrete. *Structural Concrete*, 3, 133-141.
3. Zernike, F. (1934). Beugungstheorie des Schneidenverfahrens und seiner verbesserten Form, der Phasenkontrastmethode. *Physica 1*, 689-704.
4. Raffel, M., Willert, C. and Kompenhans, J. (1998). *Particle Image Velocimetry*. Springer.
5. White, D. J. and Bolton, M. D. (2004). Displacement and strain paths during plane-strain model pile installation in sand. *Geotechnique*, 54(6), 375-397.
6. Cao, J. (2009). The shear behaviour of the reinforced concrete four-pile caps. *PhD Thesis, University of Southampton, UK.*
7. White, D. J., Take, W. A. and Bolton, M. D. (2003). Soil deformation measurement using particle image velocimetry (PIV) and photogrammetry. *Geotechnique*, 53(7), 619–631
8. White, D. J. (2002). An investigation into the behaviour of pressed-in piles. *PhD Thesis, University of Cambridge*.
9. White, D. J., Randolph, M., and Thompson, B. (2005). An image-based deformation measurement system for the geotechnical centrifuge. *IJPMG-International Journal of Physical Modelling in Geotechnics*, 1-12.
10. Cao, J. and Bloodworth, A.G. (2010), "Shear behaviour of reinforced concrete pile caps under full-width wall loading." *Proceedings of the ICE - Structures and Buildings*.
11. Bloodworth, A.G., Cao, J. and Xu, M. (2010). Numerical modelling of shear behaviour of reinforced concrete pile caps. *ASCE Journal of Structural Engineering Vol. 138 Issue 6.*
12. Walkden, E .and Bloodworth, A. (2016). Visualization of fresh cut timber deformation by photogrammetry. *ASCE Journal of Engineering Mechanics Vol. 143 Issue 4*.

Table 1 IA and SA array parameters applied to experimental samples in Batches 3 and 4

	IA size	IA spacing	SA size
Batch 3	20 x 20 pixels	16 pixels	60 x 60 pixels
Batch 4	20 x 20 pixels	16 pixels	40 x 40 pixels

Table 2 Pre-test showing mean and STD of *U'*, *V'* for B4B3 with combinations of IA and SA size (Real $V' = -5.5477$ pixels, $U' = 0$ pixels)

IA size (pixels)	SA size (pixels)	*U'* (pixels)		*V'* (pixels)	
		Mean	STD	Mean	STD
20	10	-0.150094	0.068549	-5.91694	0.0432152
20	60	-0.148278	0.068954	-5.91605	0.0432197
40	10	-0.150675	0.054549	-5.91676	0.0263482
40	60	-0.150217	0.052721	-5.91822	0.0257143
60	10	-0.151664	0.052861	-5.91771	0.0220514
60	60	-0.149878	0.053501	-5.91688	0.0224614

Table 3 Pre-test showing mean and STD of random strain ε_{xx}, ε_{yy} for B4B3 with combinations of IA and SA size
(real $\varepsilon_{xx} = 0$, $\varepsilon_{yy} = 0$)

IA size (pixels)	SA size (pixels)	ε_{xx} (με)		ε_{yy} (με)	
		Mean	STD	Mean	STD
20	10	-8.47	1080	-0.088	830
20	60	-9.13	1070	-0.085	840
40	10	-12.0	689	-1.650	410
40	60	-13.9	666	-1.980	380
60	10	-15.2	629	0.014	270
60	60	-15.0	625	-0.004	-5.87E-21

Table 4 System error correction factor r_v (= r_u)

Pile cap ref.	IA size (pixels)			Mean r_v used
	20	40	60	
B4A1	1.020	1.020	1.020	1.020
B4A2	0.948	0.949	0.948	0.949
B4A3	1.002	1.007	1.006	1.005
B4A4	0.876	0.958	0.958	0.931
B4A5	0.923	0.926	0.925	0.925
B4B2	0.988	0.988	0.988	0.988
B4B3	0.936	0.936	0.936	0.936

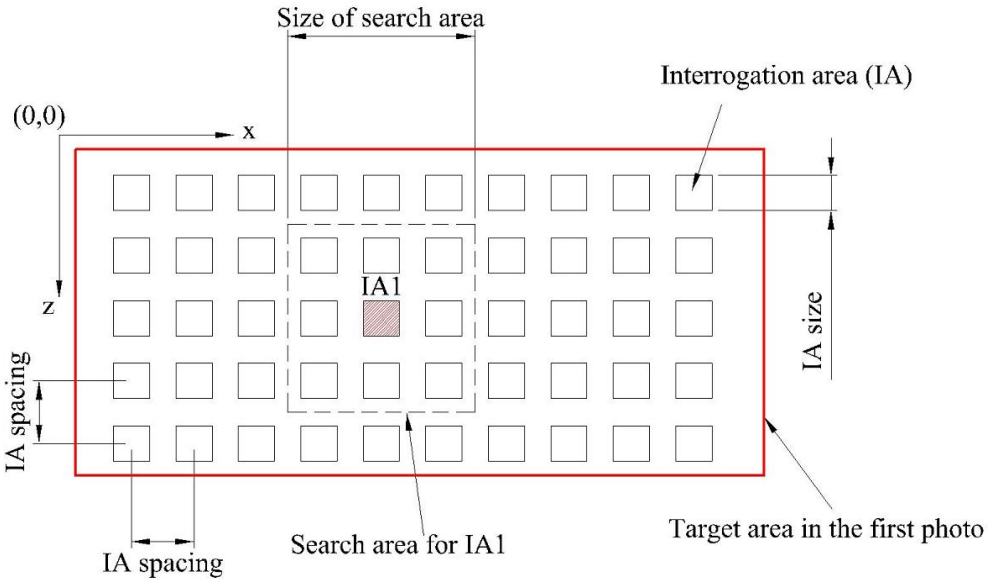

Figure 1 PIV principles: target area, IA array and search area

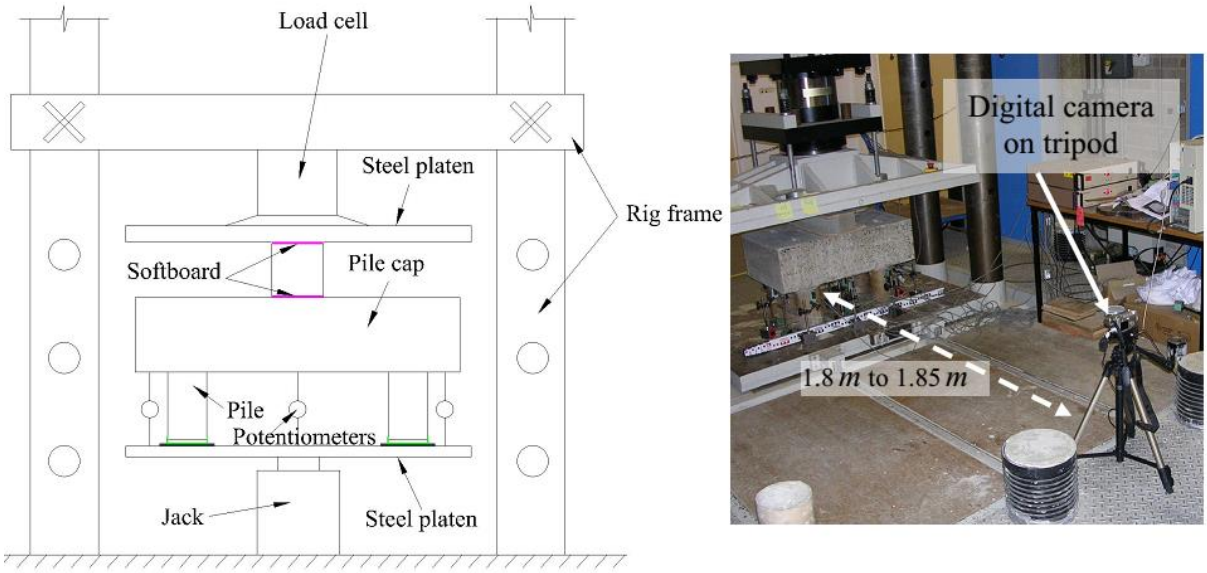

(a) Pile cap loading arrangement (b) Positioning of digital camera

Figure 2 Pile cap shear experiments at Heavy Structures Laboratory at University of Southampton, the UK

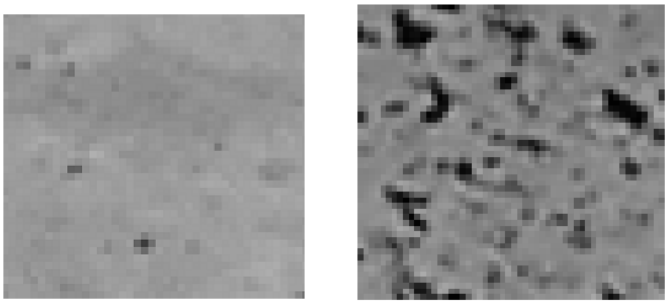

(a) Natural concrete surface (b) Concrete surface after black paint application

Figure 3 Texture of surface colouration on concrete (50x50 pixel area)

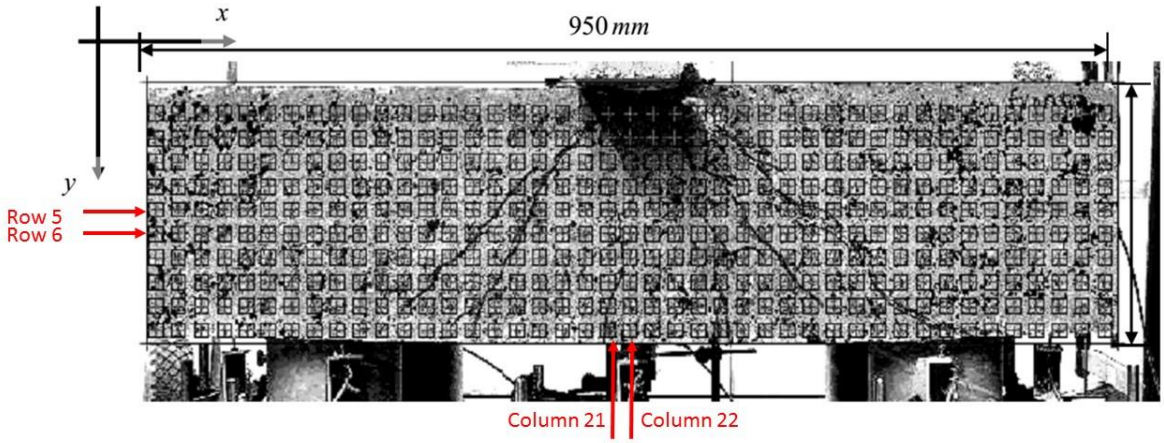

Figure 4 Co-ordinate system and IA array for cap B4B3 in pre-test (IA size of 10 pixels with IA spacing of 16 pixels)

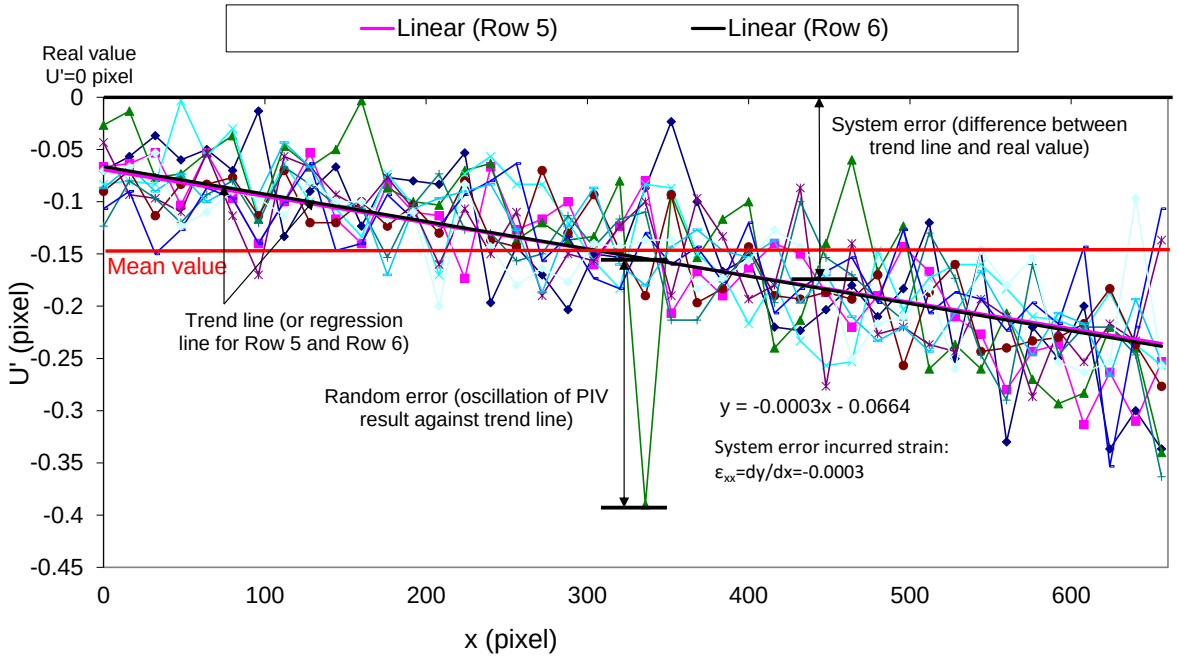

Figure 5 Horizontal displacement *U'* in pixels in pre-test for cap B4B3 (IA size of 10 pixels with IA spacing of 16 pixels)

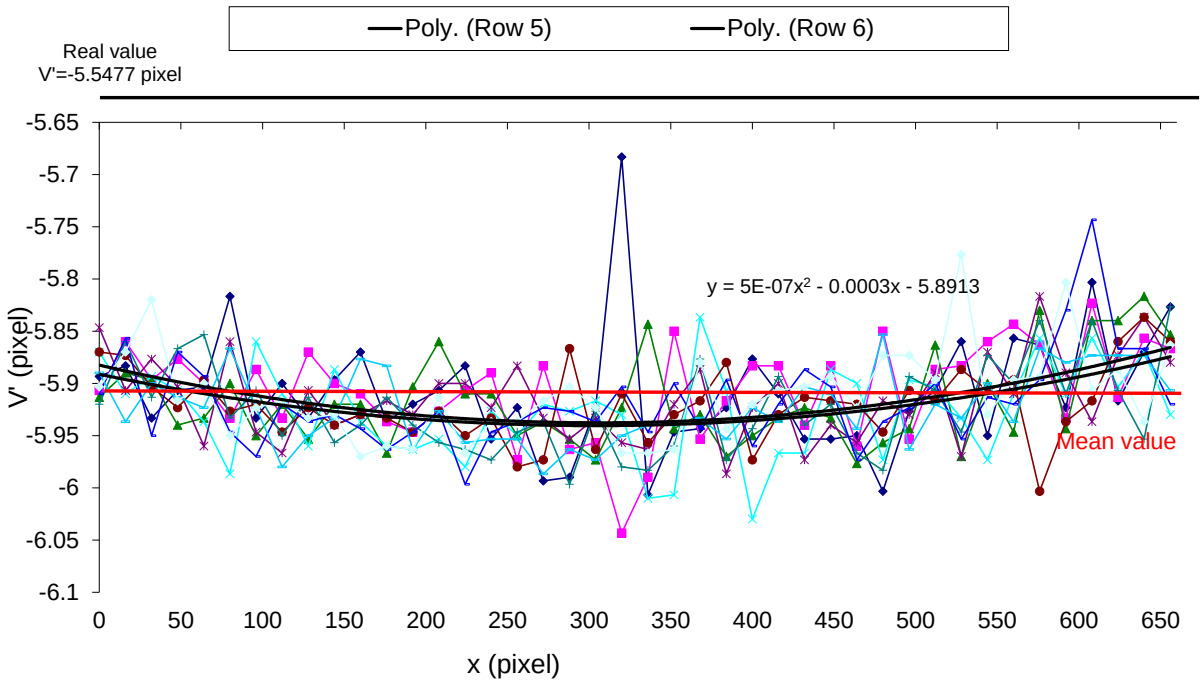

Figure 6 Vertical displacement *V'* in pixels in pre-test for cap B4B3 (IA size of 10 pixels with IA spacing of 16 pixels)

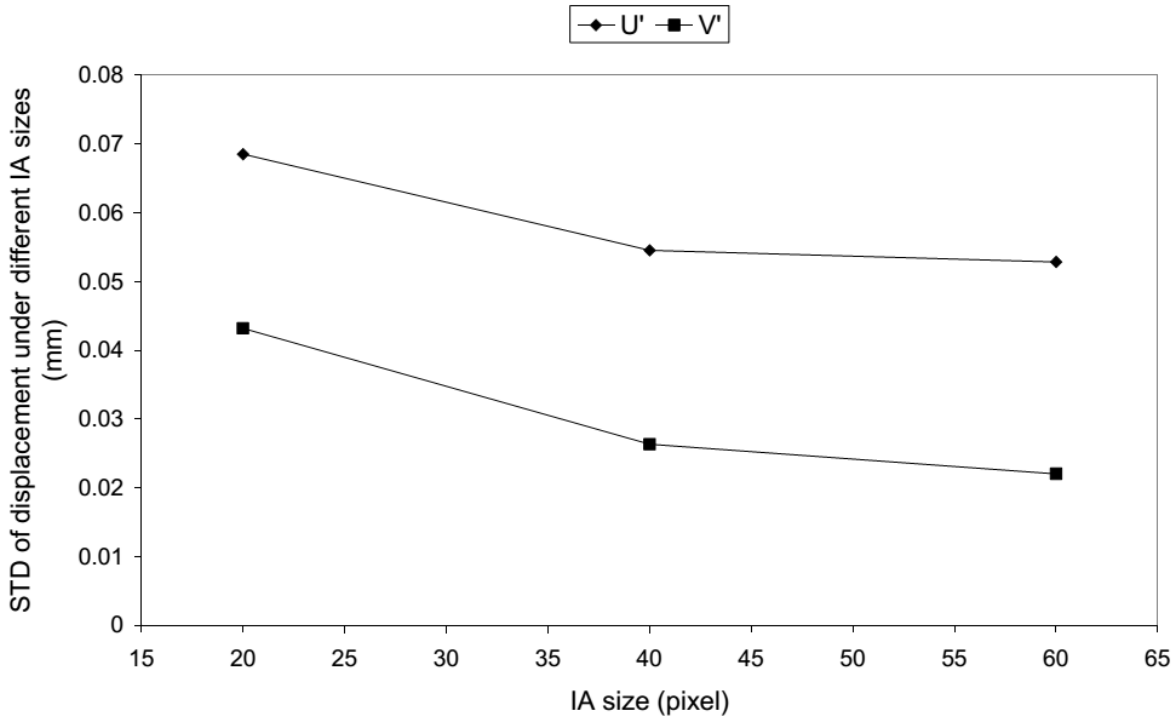

Figure 7 Variation of random error incurred displacement *U',V'* against IA size in pre-tests (SA 10 pixels) for cap B4B3

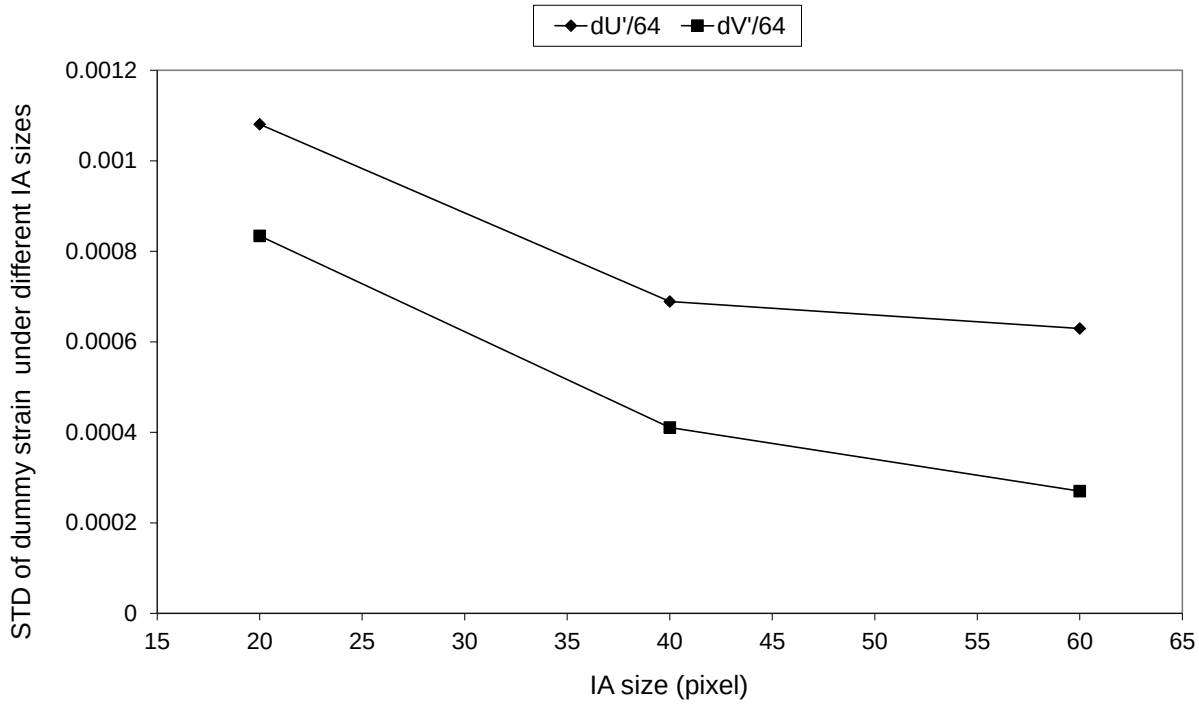

Figure 8 Variation of random error incurred strain $\varepsilon_{xx}, \varepsilon_{yy}$ against IA size in pre-tests (SA 10 pixels) for cap B4B3

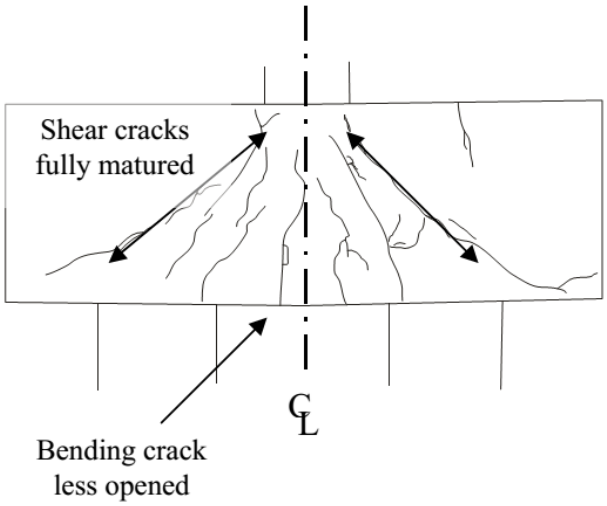

Figure 9 Observed crack pattern for cap B4A5 at shear failure

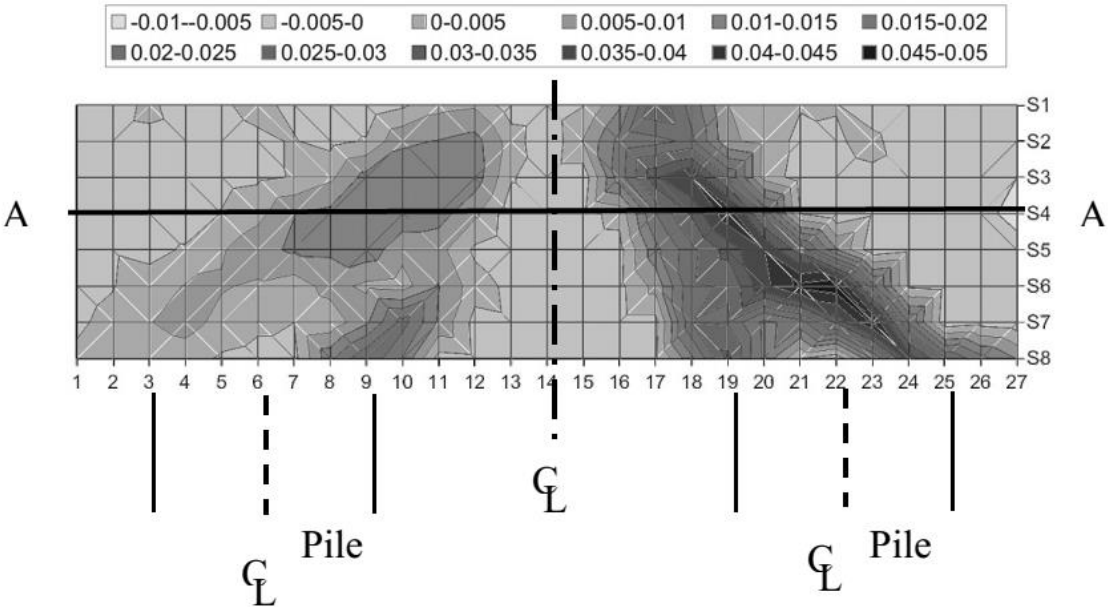

Figure 10 Contour of maximum principal strain ε_1 from PIV for cap B4A5 at shear failure

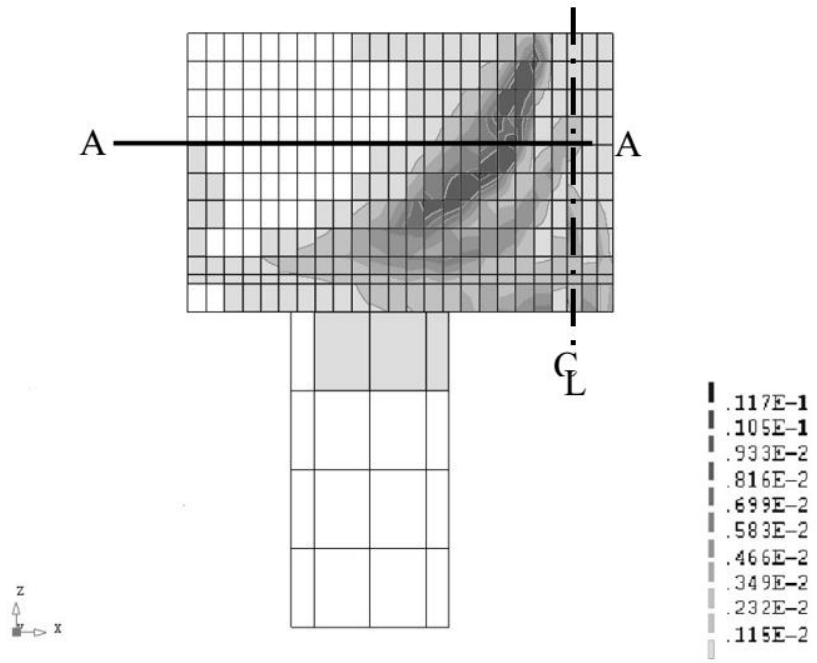

Figure 11 Crack strain ε^{cr} from smear crack based FEA for cap B4A5 at shear failure (half cap)

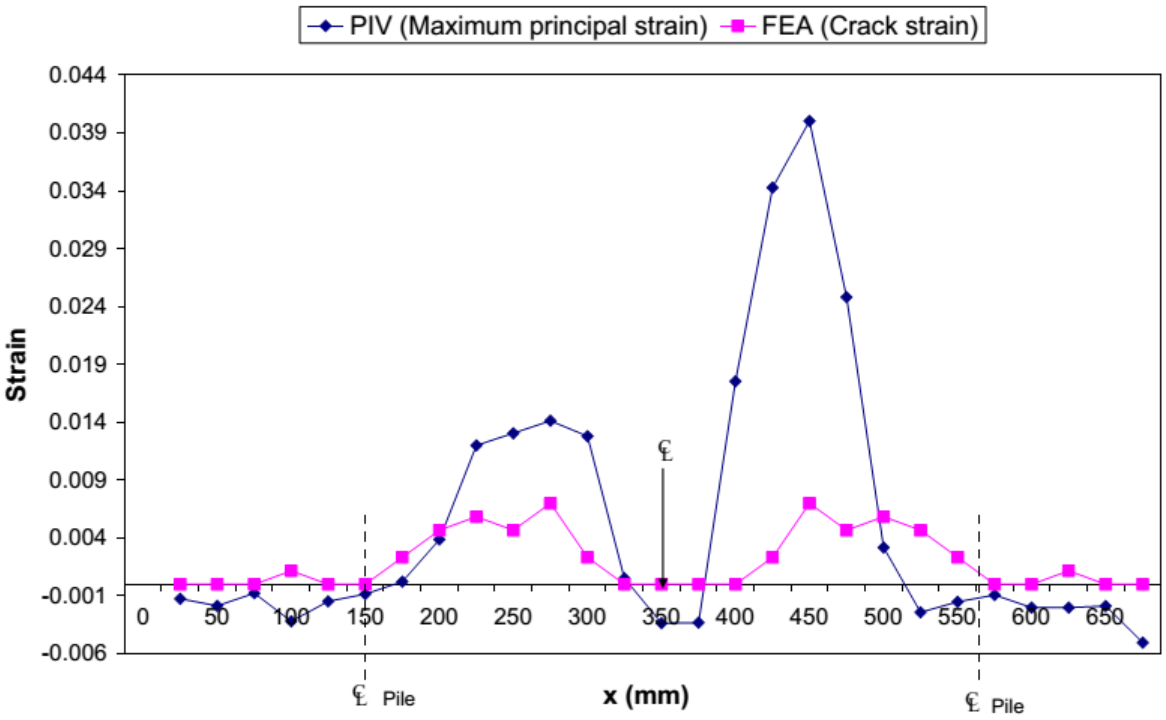

Figure 12 Comparison of maximum principal strain ε_1 between PIV and FEA for cap B4A5

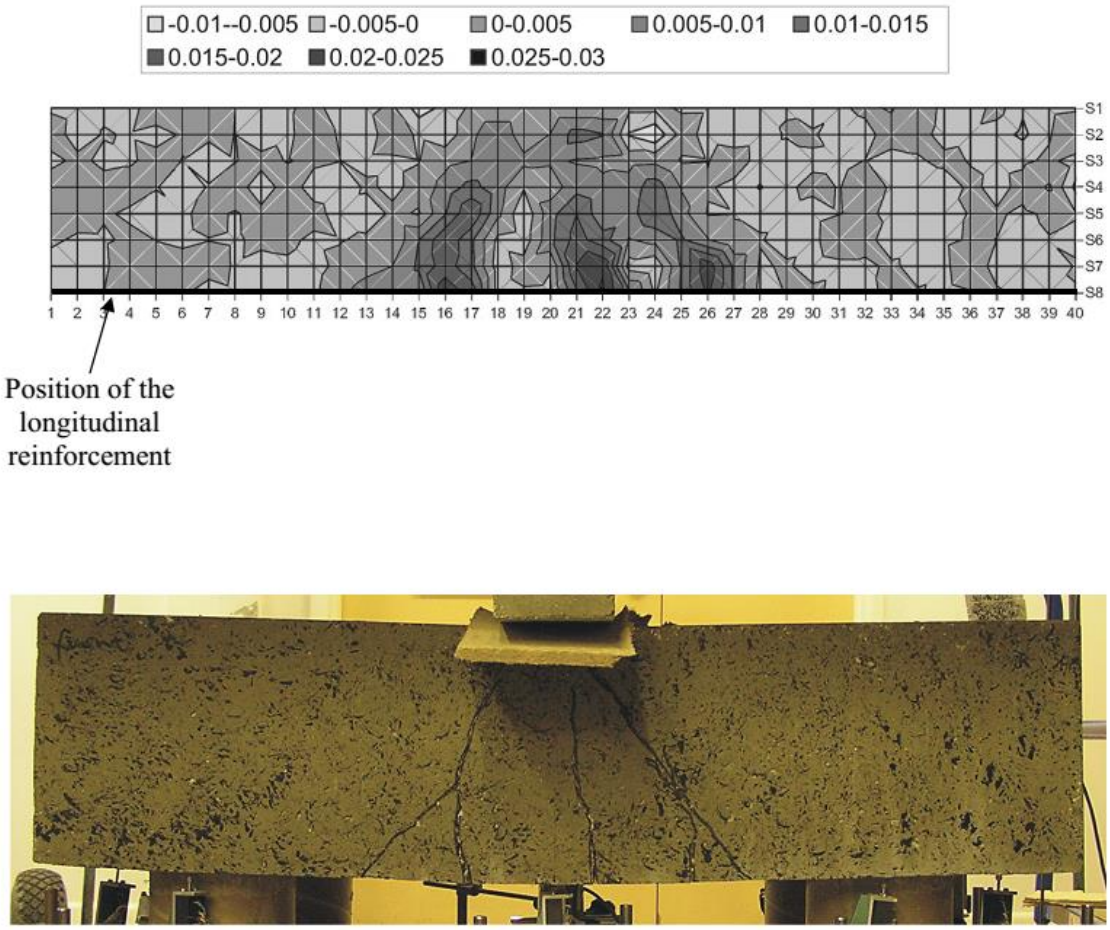

Figure 13 Contour of maximum horizontal strain ε_{xx} from PIV (above) for cap B4B2 at failure

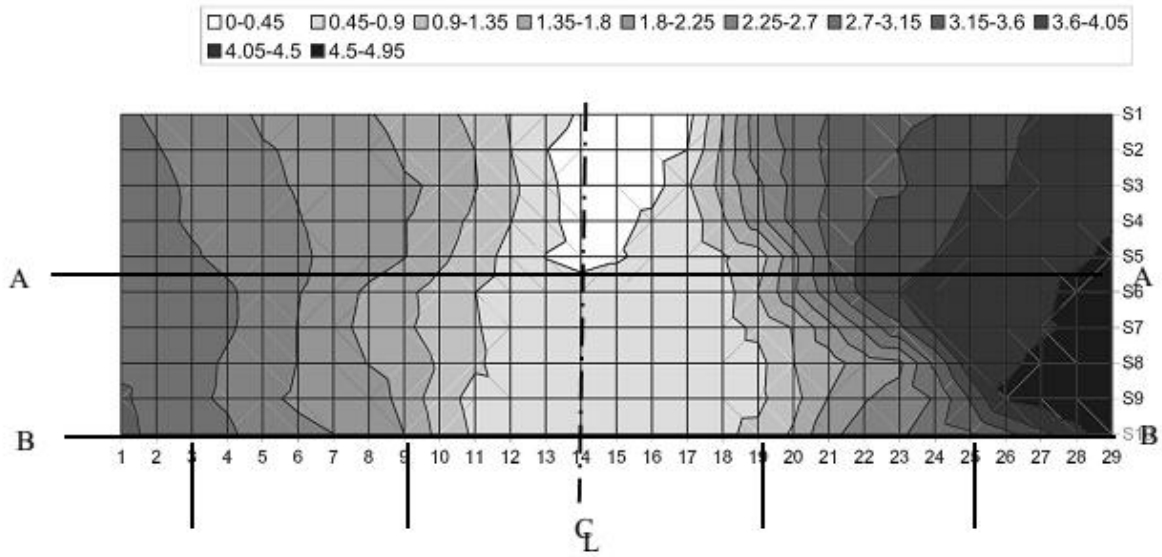

Figure 14 Resultant displacement d(mm) from PIV for cap B4A5 at shear failure

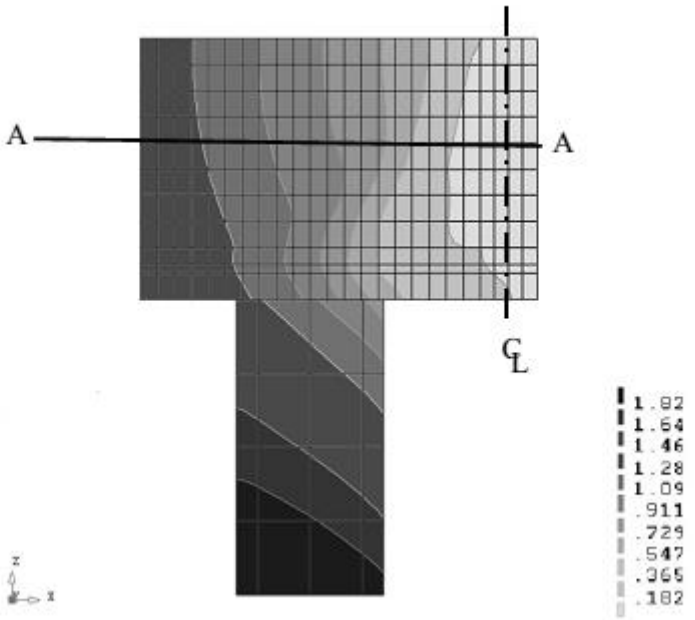

Figure 15 Resultant displacemetn d(mm) from FEA for cap B4A5 at shear failure

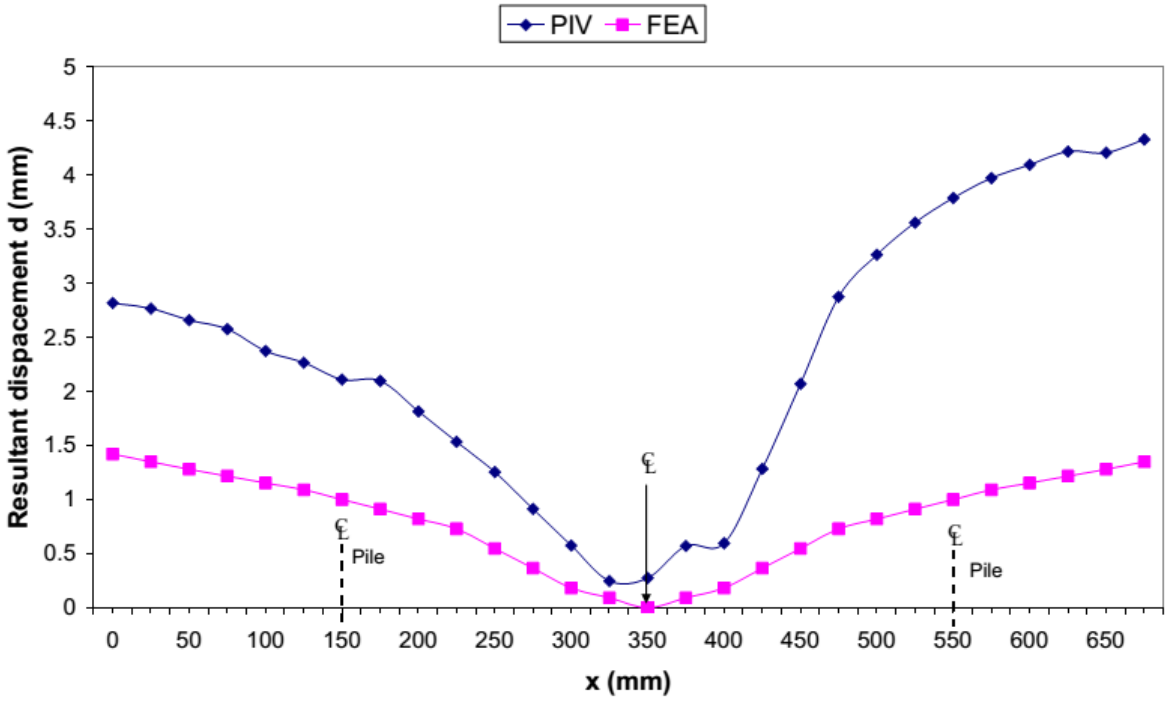

Figure 16 Comparison of d (mm) along A-A between PIV and FEA for cap B4A5 at shear failure